Thermodynamically controlled preservation of organic carbon in floodplains

Kristin Boye[1,2]*, Vincent Noël[1], Malak M. Tfaily[3], Sharon E. Bone[1], Kenneth H. Williams[4], John R. Bargar[1] and Scott Fendorf[2]

Organic matter decomposition in soils and terrestrial sediments has a prominent role in the global carbon cycle. Carbon stocks in anoxic environments, such as wetlands and the subsurface of floodplains, are large and presumed to decompose slowly. The degree of microbial respiration in anoxic environments is typically thought to depend on the energetics of available terminal electron acceptors such as nitrate or sulfate; microbes couple the reduction of these compounds to the oxidation of organic carbon. However, it is also possible that the energetics of the organic carbon itself can determine whether it is decomposed. Here we examined water-soluble organic carbon by Fourier-transform ion-cyclotron-resonance mass spectrometry to compare the chemical composition and average nominal oxidation state of carbon—a metric reflecting whether microbial oxidation of organic matter is thermodynamically favourable—in anoxic (sulfidic) and oxic (non-sulfidic) floodplain sediments. We observed distinct minima in the average nominal oxidation state of water-soluble carbon in sediments exhibiting anoxic, sulfate-reducing conditions, suggesting preservation of carbon compounds with nominal oxidation states below the threshold that makes microbial sulfate reduction thermodynamically favourable. We conclude that thermodynamic limitations constitute an important complement to other mechanisms of carbon preservation, such as enzymatic restrictions and mineral association, within anaerobic environments.

Soils and terrestrial subsurface sediments host the largest dynamic carbon (C) stock on Earth, 3,500 to 4,800 Pg (ref. 1). A large fraction of this C exists in environments where anoxic conditions are common, such as wetlands (500–700 Pg) and peatlands (~1,700 Pg) (ref. 1). Increasing evidence suggests that organic matter stored in environments where oxygen limitations occur contribute appreciably to global C cycles[2–5]. Moreover, soluble C exported from anoxic sediments has been posited to drive biogeochemical cycles in downstream aquatic systems[6]. This warrants further elucidation of controls on C cycling and the composition of soluble C in oxygen-depleted environments to accurately estimate global C dynamics.

Here we report results from an examination of the chemical composition of water-soluble organic matter in relation to the prevalent redox regime in subsurface sediment cores from four floodplains within the upper Colorado River Basin, USA (Supplementary Table 1). Building on a thermodynamic framework[7,8], we posit that C preservation in anoxic environments is linked to energetic constraints on microbial metabolic activity disabling the oxidation of highly reduced C compounds. Microorganisms generally require organic substrates to be solubilized to metabolize them[9]. Multiple mechanisms regulate solubilization of organic compounds, including exo-enzymatic activity[10], association with minerals[11], and hydrophobicity[11,12]. For the water-soluble fraction available to microorganisms, C mineralization is constrained by a thermodynamic threshold established by the electron acceptor[6]. Thus, thermodynamic limitations act as an additional thresholding mechanism, preventing microorganisms from using solubilized C substrates if they provide insufficient energy to sustain microbial growth in the prevailing redox regime[7,13]. Therefore, thermodynamic preservation of water-soluble C in anaerobic soils/sediments should result in a skewing of the relative compound class distribution towards water-soluble C compounds with a nominal oxidation state of carbon (NOSC) that reside below the thermodynamic threshold. Because the water-soluble fraction represents organic C, that is, or has been, available for microbial respiration, we posit that thermodynamically favourable substrates (higher NOSC) are removed, whereas unfavourable compounds (lower NOSC) remain. Thus, thermodynamic limitation should lead to a successional decrease in the average NOSC of water-soluble C compounds. To test this hypothesis, we compare Fourier-transform ion-cyclotron-resonance mass spectrometry (FT-ICR-MS) data for water extracts from sediments exhibiting anaerobic, sulfate-reducing conditions (sulfidic) with data from sediments with aerobic conditions (non-sulfidic) across all four floodplains.

Floodplains constitute one of the most widely distributed terrestrial environments associated with sediment burial, organic-rich deposits, and anoxic conditions[14–18]. Our sites exhibit highly heterogeneous stratigraphy produced by active river meandering and sediment burial; dominant coarse-grained materials are interspersed with finer-grained sediments and co-deposited organic matter, leading to distinct zones of oxic or anoxic conditions within the subsurface. In general, aerobic respiration can be assumed to dominate above the groundwater table and in coarse-grained, low-C materials in the water-saturated zone, where the inflow of oxygen is fast enough to compensate for respiratory consumption (Fig. 1a). However, in high-C materials below the groundwater table, higher oxygen consumption rates and limited supply are
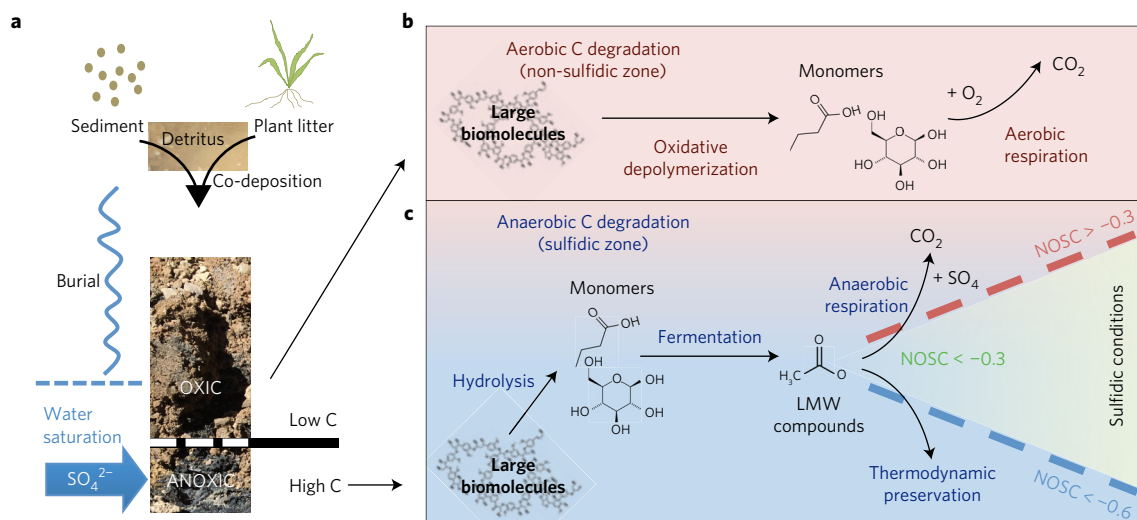
415

Figure 1 | Conceptual model of the evolution of anaerobic environments and thermodynamic constraints on carbon (C) fate in the subsurface of floodplains. a–c, The degradation of organic matter that was co-deposited with sediment (**a**) proceeds without thermodynamic limitations in oxic zones (unsaturated zone and low-C sediments in the water-saturated zone) (**b**). Anoxic conditions develop where C concentration is high in the water-saturated zone. With sulfate as the dominant electron acceptor, only low-molecular-weight (LMW) substrates with a nominal oxidation state of C (NOSC) above the thermodynamic limit (−0.6 at standard state conditions, −0.3 at sulfidic conditions) are energetically viable for respiring microorganisms (**c**).

likely to induce anaerobic conditions. Because sulfate concentrations are high (4–100 mM) in the groundwater at these sites, sulfate respiration is the dominant metabolic pathway in the absence of oxygen, and iron sulfides are abundant in water-saturated organic-rich deposits[19]. Therefore, to simplify the comparisons with aerated environments, we only considered the energetics of sulfate as terminal electron acceptor (TEA) in our thermodynamic calculations. To this end, we used authigenic iron sulfides, which are produced as a consequence of sulfate respiration, sensitive to oxidation, and with relatively low solubility, as indicators of where sulfate reduction is prevalent in the natural setting, thus allowing us to probe the long-term effect on organic matter preservation and composition. Sedimentary sulfides were identified by sulfur X-ray absorption near-edge structure (XANES) spectroscopy (Supplementary Fig. 1).

Theoretical framework for thermodynamic C preservation

Anaerobic decomposition of organic matter is generally considered to proceed at slower rates than aerobic decomposition due to reliance on hydrolytic enzymes for depolymerization of macromolecules; fermentation being a slower process yielding less energy than respiration; and lower energy yields for anaerobic than aerobic respiration[9]. Thermodynamic descriptions of heterotrophic respiration traditionally account for differences in energy yield based on available TEAs (refs 20–22). This approach fails to consider the energy limitations placed on the oxidation half-reaction and the relevance of the type of C substrates available to act as electron donors. Oxygen reduction yields around −118 kJ mol^{-1} e^{-} transferred, which appreciably overrides variation in electron donor energetics in aerobic metabolism. Consequently, aerobic decomposition rates can be considered to be kinetically controlled[7]. With sulfate as the TEA, however, the energy gain from the metabolic reactions approaches the energy required to sustain growth[7]. Hence, the energy cost of the oxidation half-reaction must be accounted for and coupled with the electron acceptor half-reaction to predict microbial energy yields and respiration rates[13].

For natural organic matter, the energy cost for oxidation of organic C to CO_2 can be estimated through an inverse linear relationship between the Gibbs free energy of oxidation (ΔG_{ox}) and the nominal oxidation state of carbon (NOSC)[13], which can

be calculated based on the elemental stoichiometry of the organic matter molecular composition (see Methods)[13]. Based on this relationship, the thermodynamic limit for organic matter respiration with specific TEAs can be estimated. Here, we focus on comparing oxygen as the dominant TEA in non-sulfidic zones to sulfate as the dominant TEA in sulfidic zones. According to calculations based on pore-water data from the Rifle site, the thermodynamic limit for sulfate reduction occurs when NOSC < −0.3 at current conditions within the sulfidic samples, or when NOSC < −0.6 assuming standard state conditions (see Methods and Supplementary Tables 2 and 3). Thus, thermodynamic constraints indicate that microbial respiration with sulfate would selectively oxidize water-soluble C substrates with a NOSC above the threshold value. This would progressively shift the average NOSC of the entire water-soluble C pool towards more negative values for sediments sustained under sulfate-reducing conditions. Conversely, in non-sulfidic zones, thermodynamic limitations to C oxidation do not apply with respect to NOSC, thus maintaining a higher average NOSC within these samples (Fig. 1b,c).

Field evidence of thermodynamic C preservation

Our investigations revealed a clear trend of more reduced C (more negative average NOSC) in sulfidic zones than in non-sulfidic sediments at all sites (Figs 2 and 3a and Supplementary Fig. 2a). Although all samples were taken below the annual maximum water table level, where water-saturated conditions occur, sulfides were exclusively found in sections of the core with the highest C concentration (Fig. 2). These samples also exhibited a greater ratio of reduced (Fe(II)) to oxidized (Fe(III)) iron (Supplementary Fig. 2c,d), indicating that pronounced reducing conditions develop only where organic matter concentrations are high enough to support microbial oxygen consumption beyond repletion rates. Consequently, an inverse correlation between organic C concentration and the average NOSC of water-soluble C was observed (Supplementary Fig. 2b). These zones appear to form in deposited sediments having higher organic matter content (Fig. 1a), leading to oxygen depletion and poising of the system at sulfate-reducing conditions. This in turn has caused selective depletion of water-soluble C compounds with a NOSC above the thermodynamic threshold, whereas decomposition of C in oxygenated,
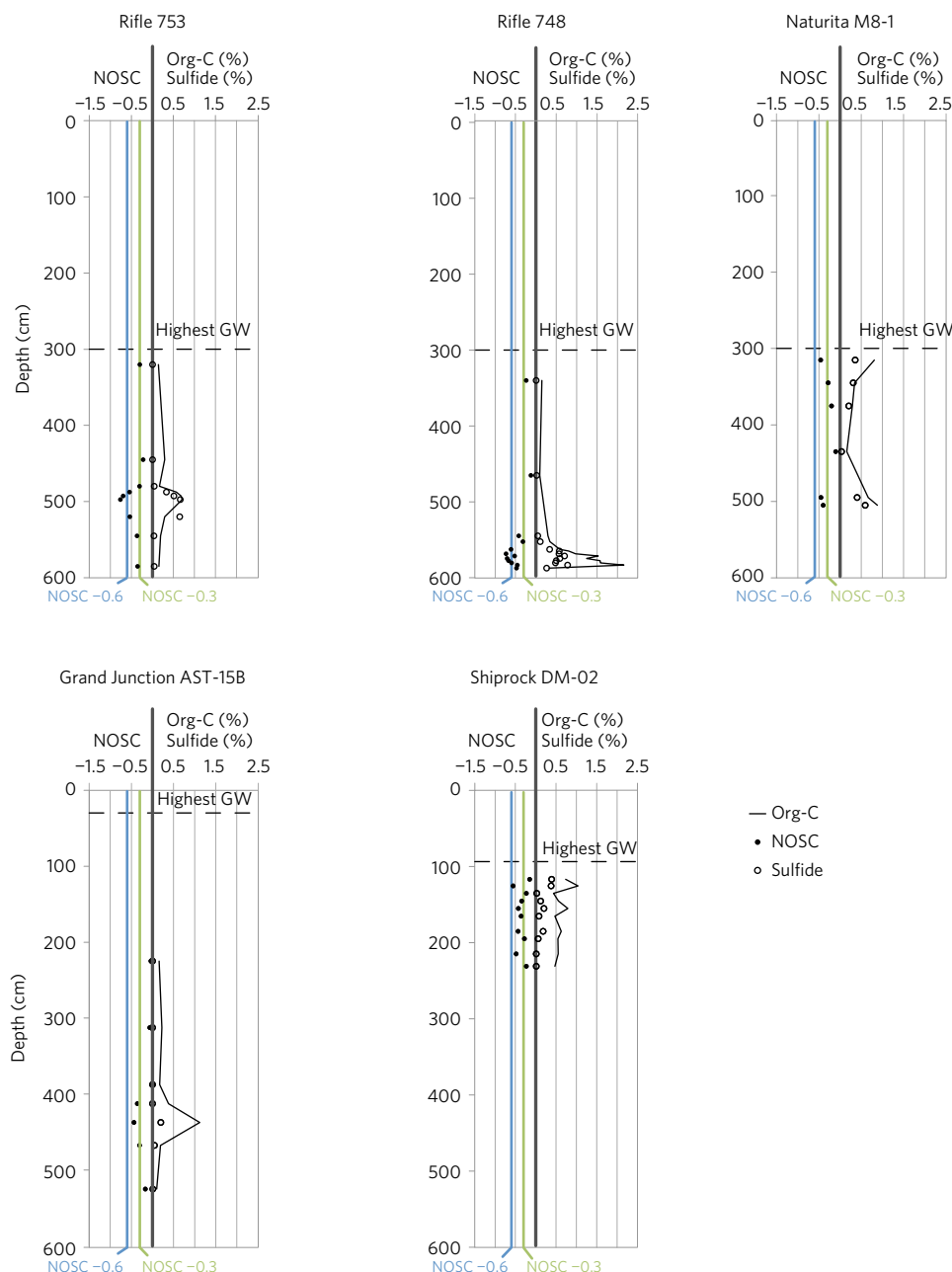
Figure 2 | Sediment profiles of the five examined cores from the four floodplains in the Upper Colorado River Basin, USA. Authigenic sulfides (open circles, % of sediment dry weight) co-occur with an increase in organic C (Org-C, thick black line, % of sediment dry weight) and lower NOSC (filled black circles) below the annual maximum groundwater level (dashed black line) at all sites. The thermodynamic limits for organic C oxidation coupled to sulfate reduction at standard state (NOSC < −0.6) and at sulfidic (NOSC < −0.3) conditions are depicted by blue and green solid lines, respectively.

non-sulfidic zones can transpire without exceeding thermodynamic constraints imparted by the C compounds and, consequently, without selectivity based on the NOSC. Presumably, the lack of thermodynamic limitations leads to faster C turnover rates in non-sulfidic zones, although without time-resolved data we cannot determine the effect on overall C fluxes. However, the distinction in average NOSC of soluble organic C between sulfidic and non-sulfidic samples (Fig. 3a) clearly indicates that thermodynamic constraints are operational within sulfidic zones of these floodplains.

A relative distribution between different chemical classes can be approximated by grouping FT-ICR-MS-identified molecules based on their O/C and H/C elemental ratios (Supplementary Table 4)[23–25]. Each chemical class contains compounds with a

wide range of NOSC, but the average NOSC of a class illuminates an implicit link between NOSC and chemical composition (Supplementary Figs 3–5). Thus, higher abundance of proteinaceous (average NOSC = −0.9) and lipid-like (average NOSC = −1.3) compounds in a sample is reflected in a lower average NOSC, whereas carbohydrates (average NOSC = +0.1) and aromatics (average NOSC for lignin-like and tannin-like compounds was −0.3 and +0.8, respectively) shift the average NOSC of a sample to higher values. Indeed, our sulfidic samples contained a larger fraction of proteinaceous compounds than the non-sulfidic samples, and a similar pattern was discerned for lipid-like compounds (Fig. 3b and Supplementary Figs 3–5). This is consistent with the observed lower average NOSC for sulfidic samples and with previous observations of aliphatic compounds being relatively
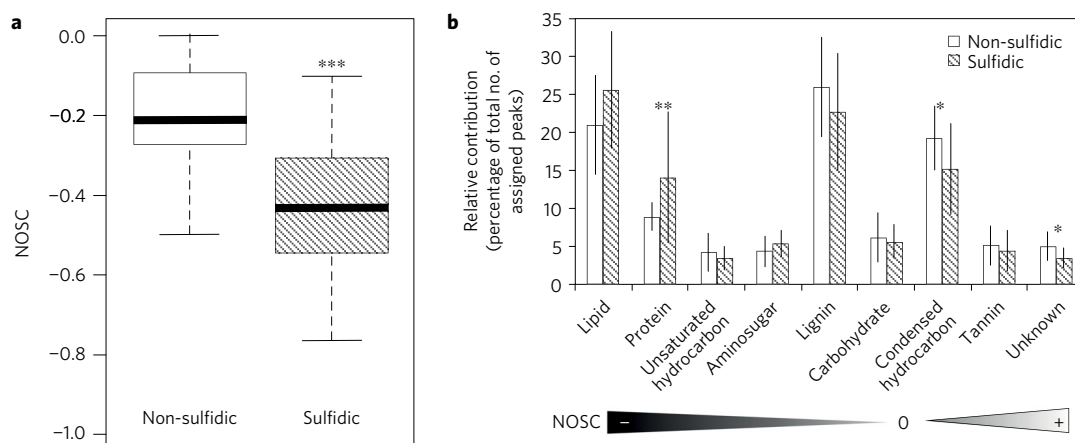
Figure 3 | Chemical signature induced by thermodynamic constraints on C oxidation in sulfidic samples acting to selectively preserve highly reduced C.
a, Box–whisker plot showing the average NOSC of water-soluble compounds was lower in sulfidic samples. **b**, Average relative distribution between C compound classes in non-sulfidic and sulfidic samples (average NOSC increases from left to right). Error bars denote standard deviation of the mean. Unknowns have O/C and H/C ratios outside the limits[23-25] used to group molecular formulae. Asterisks denote significant differences between sulfidic and non-sulfidic samples according to Welch's unequal variances t-tests (*, $p < 0.05$; **, $p < 0.01$; ***, $p < 0.001$).

more abundant where oxygen is limited, such as in marine environments[26-28], wetlands[12], and in deep soil/sediments[29-31]. Preservation of proteins has previously been attributed to their specific ability to interact with mineral surfaces[11,32]. Similarly, the hydrophobic nature of lipids and other aliphatics is suggested to occlude them from the soluble fraction[11,12]. However, we observed no clear difference in the solid-phase, bulk C composition between sulfidic and non-sulfidic samples in the two cores from the Rifle site, which were selected to be examined by C near-edge X-ray absorption fine structure (NEXAFS) spectroscopy (Supplementary Figs 4 and 5). Thus, our data reveal a shift in C chemistry exclusive to the water-soluble fraction, which cannot be attributed to mineral protection or occlusion acting upon specific compounds. Moreover, the FT-ICR-MS data do not indicate increased sulfurization of organic compounds in the sulfidic sediments (Supplementary Table 5) that could explain the selective preservation of C. In fact, S-containing compounds and condensed aromatic compounds (aromaticity index, AI ≥ 0.67) (ref. 33) made up a larger fraction of the total number of compounds in non-sulfidic than in sulfidic samples. There were no clear differences between sulfidic and non-sulfidic samples in averaged aromaticity index[33], double bond equivalents, expression of specific reaction pathways (for example, hydration, oxygenation)[24], or the relative abundances of compounds containing N, S, and/or P (Supplementary Table 5). The average concentration of water-soluble C tended to be higher in sulfidic samples (consistent with a higher total C concentration), but a greater proportion of the total organic C was water-soluble in non-sulfidic zones (Supplementary Table 5). This may indicate that additional C protection mechanisms, preventing C from entering the water-soluble fraction, are active in the sulfidic zones. Conceivably, the exudation of exo-enzymes is subdued in sulfidic sediments due to energetic limitations among microorganisms—that is, a feedback mechanism between water-soluble and solid-phase C compounds due to thermodynamic constraints.

Our findings indicate that highly reduced (low NOSC) water-soluble organic compounds are preferentially preserved in anaerobic environments because they provide insufficient energy to sustain microbial respiratory growth with available TEAs. This does not imply that compounds with a NOSC below the thermodynamic threshold are inherently resistant to microbial decomposition. Rather, it is the combination of environmental conditions and bioenergetics that prevents microorganisms from utilizing them as an energy source under the prevalent anaerobic redox regime[34].

Likewise, all compounds with a NOSC above the thermodynamic threshold may not be directly metabolized by microorganisms due to enzymatic (that is, kinetic) limitations.

Relevance of thermodynamic limitations for C cycling
In anoxic environments, the decomposition of organic matter is carried out by a multitude of organisms through several steps, the final being anaerobic respiration (Fig. 1)[9,10]. Thermodynamic constraints exert control over this final step and lead to selective degradation of small, soluble organic compounds, acting in parallel with kinetic and accessibility factors that limit decomposition rates. In this study, both the concentration and relative fraction of total water-soluble organic C with a NOSC below the thermodynamic threshold for sulfate reduction (NOSC < −0.3) were higher in the sulfidic ($51.6\,mg\,kg^{-1}$ soil or 65%) than non-sulfidic sediments ($27.3\,mg\,kg^{-1}$ soil or 45%). This difference ($24.3\,mg\,kg^{-1}$ soil) suggests that almost half (47%) of the organic C in the soluble fraction of sulfidic sediments remains due to thermodynamic constraints, and, hence, would rapidly be metabolized in the presence of oxygen (or nitrate). It further illustrates the importance of considering thermodynamic preservation on exported dissolved organic carbon (DOC); DOC transported from an anaerobic into an aerobic environment would become (thermodynamically) available for respiration and, thus, potentially stimulate biological activity. Although the implications of a thermodynamic limitation on mineralization of water-soluble C for solid-phase C remains to be investigated, our results across four field sites illuminate a mechanism for C preservation that is universally applicable to anaerobic environments and needs to be recognized.

Methods
Methods, including statements of data availability and any associated accession codes and references, are available in the online version of this paper.

References
1. Ciais, P. *et al*. in *Climate Change 2013: The Physical Science Basis* (IPCC, Cambridge Univ. Press, 2013).
2. Gurwick, N. P. *et al*. Mineralization of ancient carbon in the subsurface of riparian forests. *J. Geophys. Res.* **113**, G02021 (2008).

3. Gurwick, N. P. *et al*. Microbially available carbon in buried riparian soils in a glaciated landscape. *Soil Biol. Biochem.* **40**, 85–96 (2008).
4. Oost, K. V. *et al*. Legacy of human-induced C erosion and burial on soil–atmosphere C exchange. *Proc. Natl Acad. Sci. USA* **109**, 19492–19497 (2012).
5. Batson, J. *et al*. Soil greenhouse gas emissions and carbon budgeting in a short-hydroperiod floodplain wetland. *J. Geophys. Res.* **120**, 2014JG002817 (2015).
6. Marín-Spiotta, E. *et al*. Paradigm shifts in soil organic matter research affect interpretations of aquatic carbon cycling: transcending disciplinary and ecosystem boundaries. *Biogeochemistry* **117**, 279–297 (2014).
7. Jin, Q. & Bethke, C. M. Predicting the rate of microbial respiration in geochemical environments. *Geochim. Cosmochim. Acta* **69**, 1133–1143 (2005).
8. Keiluweit, M., Nico, P. S., Kleber, M. & Fendorf, S. Are oxygen limitations under recognized regulators of organic carbon turnover in upland soils? *Biogeochemistry* **127**, 157–171 (2016).
9. Fenchel, T., King, G. M. & Blackburn, T. H. *Bacterial Biogeochemistry* 3rd edn, 1–34 (Academic, 2012).
10. Burns, R. G. *et al*. Soil enzymes in a changing environment: current knowledge and future directions. *Soil Biol. Biochem.* **58**, 216–234 (2013).
11. Kleber, M., Sollins, P. & Sutton, R. A conceptual model of organo-mineral interactions in soils: self-assembly of organic molecular fragments into zonal structures on mineral surfaces. *Biogeochemistry* **85**, 9–24 (2007).
12. Jokic, A., Cutler, J. N., Ponomarenko, E., van der Kamp, G. & Anderson, D. W. Organic carbon and sulphur compounds in wetland soils: insights on structure and transformation processes using K-edge XANES and NMR spectroscopy. *Geochim. Cosmochim. Acta* **67**, 2585–2597 (2003).
13. LaRowe, D. E. & Van Cappellen, P. Degradation of natural organic matter: a thermodynamic analysis. *Geochim. Cosmochim. Acta* **75**, 2030–2042 (2011).
14. Chaopricha, N. T. & Marín-Spiotta, E. Soil burial contributes to deep soil organic carbon storage. *Soil Biol. Biochem.* **69**, 251–264 (2014).
15. Tockner, K. & Stanford, J. Review of: riverine flood plains: present state and future trends. *Environ. Conserv.* **29**, 308–330 (2002).
16. Lair, G. J. *et al*. How do long-term development and periodical changes of river–floodplain systems affect the fate of contaminants? results from European rivers. *Environ. Pollut.* **157**, 3336–3346 (2009).
17. Blazejewski, G. A., Stolt, M. H., Gold, A. J., Gurwick, N. & Groffman, P. M. Spatial distribution of carbon in the subsurface of riparian zones. *Soil Sci. Soc. Am. J.* **73**, 1733–1740 (2009).
18. Ricker, M. C. & Lockaby, B. G. Soil organic carbon stocks in a large eutrophic floodplain forest of the southeastern Atlantic coastal plain, USA. *Wetlands* **35**, 291–301 (2015).
19. Janot, N. *et al*. Physico-chemical heterogeneity of organic-rich sediments in the Rifle Aquifer, CO: impact on uranium biogeochemistry. *Environ. Sci. Technol.* **50**, 46–53 (2016).
20. Claypool, G. E. & Kaplan, I. R. in *Natural Gases in Marine Sediments* (ed. Kaplan, I. R.) 99–139 (Springer, 1974).
21. Froelich, P. N. *et al*. Early oxidation of organic matter in pelagic sediments of the eastern equatorial Atlantic: suboxic diagenesis. *Geochim. Cosmochim. Acta* **43**, 1075–1090 (1979).
22. Postma, D. & Jakobsen, R. Redox zonation: equilibrium constraints on the Fe(III)/SO4-reduction interface. *Geochim. Cosmochim. Acta* **60**, 3169–3175 (1996).
23. Tfaily, M. M. *et al*. Advanced solvent based methods for molecular characterization of soil organic matter by high-resolution mass spectrometry. *Anal. Chem.* **87**, 5206–5215 (2015).
24. Kim, S., Kramer, R. W. & Hatcher, P. G. Graphical method for analysis of ultrahigh-resolution broadband mass spectra of natural organic matter, the Van Krevelen diagram. *Anal. Chem.* **75**, 5336–5344 (2003).
25. Hodgkins, S. B. *et al*. Changes in peat chemistry associated with permafrost thaw increase greenhouse gas production. *Proc. Natl Acad. Sci. USA* **111**, 5819–5824 (2014).
26. Hedges, J. I. *et al*. The molecularly-uncharacterized component of nonliving organic matter in natural environments. *Org. Geochem.* **31**, 945–958 (2000).
27. Marchand, C., Albéric, P., Lallier-Vergès, E. & Baltzer, F. Distribution and characteristics of dissolved organic matter in mangrove sediment pore waters along the coastline of French Guiana. *Biogeochemistry* **81**, 59–75 (2006).
28. Seidel, M. *et al*. Biogeochemistry of dissolved organic matter in an anoxic intertidal creek bank. *Geochim. Cosmochim. Acta* **140**, 418–434 (2014).
29. Oades, J. M. The retention of organic matter in soils. *Biogeochemistry* **5**, 35–70 (1988).
30. Lorenz, K., Lal, R., Preston, C. M. & Nierop, K. G. J. Strengthening the soil organic carbon pool by increasing contributions from recalcitrant aliphatic bio(macro)molecules. *Geoderma* **142**, 1–10 (2007).
31. Rumpel, C. & Kögel-Knabner, I. Deep soil organic matter—a key but poorly understood component of terrestrial C cycle. *Plant Soil* **338**, 143–158 (2010).
32. Rillig, M. C., Caldwell, B. A., Wösten, H. A. B. & Sollins, P. Role of proteins in soil carbon and nitrogen storage: controls on persistence. *Biogeochemistry* **85**, 25–44 (2007).
33. Koch, B. P. & Dittmar, T. From mass to structure: an aromaticity index for high-resolution mass data of natural organic matter. *Rapid Commun. Mass Spectrom.* **20**, 926–932 (2006).
34. Schmidt, M. W. I. *et al*. Persistence of soil organic matter as an ecosystem property. *Nature* **478**, 49–56 (2011).

Acknowledgements

Author contributions

Additional information

Competing financial interests

The authors declare no competing financial interests.

Methods

Field sites, sample collection. To determine the influence of redox regime on organic matter composition, we examined sediments from four floodplains across the Upper Colorado River Basin, USA (Supplementary Table 1). We targeted sediment depth-profiles exhibiting anoxic , sulfidic zones, while accounting for stratigraphic variation (Supplementary Fig. 6). Sediment cores were obtained through rotosonic drilling (Rifle) or push coring (Grand Junction, Naturita, Shiprock) and retrieved in 1-m-long sections contained in N_2-purged plastic sleeves. The core sections were subsampled on-site in 2.5–30 cm increments depending on visible heterogeneity of the material and redox conditions (for example, textural and/or colour changes). Sediment was collected in airtight glass jars, shipped on ice, and kept at 2–4 °C. Jars with samples from the saturated zone were submerged in groundwater before capping to ensure no air was left in the jars. For reduced sediments (exhibiting a sulfidic smell and/or grey/black coloration) a small subsample for sulfur (S) speciation was obtained under N_2 or Ar flow and preserved in N_2- or Ar-purged serum vials (crimp-sealed with rubber stoppers) to minimize oxygen exposure.

Sediment characterization. The samples were dried at room temperature in an oxygen-free atmosphere (95% N_2, 5% H_2) inside a glove bag. Sample preparation for S speciation analyses was carried out in the glove bag. The samples were homogenized, sieved (1 mm), and finely ground. Total S concentration was analysed with X-ray fluorescence (XRF) spectrometry (Spectro Xepos HE). Organic C content was determined on a 200 mg subsample where carbonate C had been removed by adding aliquots of 1 ml 1M HCl for >1 h until effervescence was undetectable. The remaining solution was decanted, sediments were dried at 30 °C and homogeneously mixed prior to analysis with a Carlo Erba NA1500 elemental analyser.

Solid-phase sulfide content was analysed through S K-edge XANES spectroscopy at the Stanford Synchrotron Radiation Lightsource (SSRL) beam line 4-3 equipped with a Si(111) double-crystal monochromator. Thiosulfate was used for energy calibration (K-edge = 2,472.02 eV). Spectra (2,440–2,600 eV) were collected under He atmosphere at room temperature in fluorescence mode using a SiLi Vortex detector. For each sample six XANES spectra were averaged and the composite spectrum was normalized to an edge-step of 1 at 2,490 eV, using the Athena software[35]. No beam damage was detected when comparing separate scans of the same sample. Self-absorption was considered to be minimal, owing to finely ground samples with a total S concentration <2% (ref. 36). Sulfur speciation was determined through linear combination least-squares (LC-LS) fitting using reference spectra collected under the same conditions as the sample spectra. The reference library consisted of potassium sulfate (K_2SO_4), sodium thiosulfate ($Na_2S_2O_3$), pyrite (FeS_2), synthetic greigite (Fe_3S_4), mackinawite ($Fe_{1+x}S$), elemental sulfur (S^0), marcasite (FeS_2), pyrrhotite ($Fe_{1-x}S$), and polysulfides. Linear coefficients were constrained only to be positive. The quality of LC-LS fits was estimated by an R-factor, $Rf = \sum(c_{exp} - c_{calc})^2 / \sum(c_{exp})^2$, with c_{exp} and c_{calc} referring to the measured and calculated intensity, respectively. The accuracy of this fitting procedure ranged between ±25% and ±5% of the stated values for each individual contribution, and contributions below 10% were considered as not statistically significant[36,37]. Example fits for one non-sulfidic and one sulfidic sample are shown in Supplementary Fig. 5. Total sulfide concentrations were calculated for each sample by multiplying the total S concentration of the sample by the sum of the relative proportions of pyrite, mackinawite, greigite, and elemental S.

The ratio of Fe(II) to Fe(III) in the solid phase of sediment samples analysed for sulfide was determined based on Fe K-edge X-ray absorption near-edge structure (XANES) spectroscopy. Fe XANES spectra were collected at SSRL beam line 4-1, operating in transmission mode and using a Si(111) double-crystal monochromator. To strictly preserve the oxidation state of iron during these analyses, all sediment samples were mounted on the cryostat sample rod within a glove bag and carried to the beam line in a liquid nitrogen bath before being rapidly transferred into the liquid He cryostat (temperature = 10 K). No beam damage was detected in between the different scans. Energy was calibrated by Fe metal foil (7,112 eV). For each sediment sample, 6–10 scans were recorded, depending on the concentration (1 and 3 wt% Fe) and speciation of Fe. Linear combination least-squares (LC-LS) fitting of the Fe XANES was performed in Athena as described for S XANES, using a large set of natural and synthetic model compounds[38].

Solid-phase C chemistry was examined by C K-edge near-edge X-ray absorption fine structure (NEXAFS) in select samples from the two sediment cores from Rifle. Data was collected at the SGM 11ID-1 beamline at the Canadian Lightsource. The X-ray energy was calibrated with citrate (288.7 eV) (ref. 39) and sample spectra were normalized by subtracting the baseline (265–270 eV) fluorescence to obtain 0 intensity in the pre-edge region, dividing by Au reference spectra (average of >100 scans on clean gold foil), and edge-normalization (step height = 1, I0 = 290 eV, pre-edge = 270–275 eV, post-edge = 310–318 eV) performed in Athena (iXAFS v 2.2). The peak fitting was carried out by the deconvolution option in Athena (iXAFS v 2.2) with Gaussian peaks assumed to

correspond to the following functionalities: quinonic C (284.05 eV), aromatic C (285.1 eV), phenol-C (286.3 eV), aliphatic C (287.5 eV), carboxyl-/amide-C (288.6 eV), O-alkyl C (289.5 eV), and carbonate (290.3 eV). To optimize the fits, the full-width at half-maximum (FWHM) was allowed to vary between 0.3–0.5 and the peak energy was varied within the published ranges for peak energies of reference compounds[39–41]. Once optimized for our sample set, the same settings for FWHM and peak energy were used for the fitting of all sample spectra. In addition to the $1s$-π^* transitions represented by the Gaussians, we used an arc tangent function (290 eV, FWHM = 0.3, height = 1) to represent the edge-step and two broad (FWHM = 3) Gaussian functions at 292 eV and 300 eV to represent the σ^* transitions.

Water-soluble C chemistry. Water extracts (1:10 sediment:water weight ratio) were used to examine the water-soluble organic C (that is, dissolved and soluble fraction of organic matter). Total organic C in extracts were analysed for non-purgeable organic C (NPOC) using a Shimadzu TOC-L analyser with in-line acidification (phosphoric acid) and purging of samples to drive off inorganic C.

FT-ICR-MS analyses. The chemical composition of water-soluble organic C was examined using a 12 Tesla Bruker SolariX Fourier-transform ion-cyclotron-resonance mass spectrometer (FT-ICR-MS) within the Environmental Molecular Sciences Laboratory (EMSL). Extracts were diluted 50:50 (v/v) with LC–MS grade methanol less than 30 min before analysis to minimize potential esterification. Samples were injected directly into the mass spectrometer and the ion accumulation time was optimized for all samples. A standard Bruker electrospray ionization (ESI) source was used to generate negatively charged molecular ions. Samples were introduced to the ESI source equipped with a fused silica tube (30 μm i.d.) through an Agilent 1200 series pump (Agilent Technologies) at a flow rate of 3.0 μl min^{-1}. Experimental settings followed previously established optimal parameterization: needle voltage +4.4 kV; Q1 set to m/z 50; heated resistively coated glass capillary operated at 180 °C. All samples were run with instrument settings optimized by tuning on the IHSS Suwannee River fulvic acid standard. The instrument was externally calibrated weekly with a tuning solution from Agilent, which calibrates to a mass accuracy of <0.1 ppm and contains the following compounds: $C_2F_3O_2$, $C_6HF_9N_3O$, $C_{12}HF_{21}N_3O$, $C_{20}H_{18}F_{27}N_3O_8P_3$, and $C_{26}H_{18}F_{39}N_3O_8P_3$ with an m/z range of 112–1,333. Forty-four individual scans were averaged for each sample, and they were internally calibrated using an organic matter homologous series separated by 14 Da ($-CH_2$ groups). Mass measurement accuracy was typically within 1 ppm for singly charged ions across a broad m/z range (100–1,100). The mass resolution was ~350,000 at m/z 321. All observed ions in the spectra were singly charged, as confirmed by the 1.0034 Da spacing found between isotopic forms of the same molecule (between $^{12}C_n$ and $^{12}C_{n-1}$–$^{13}C_1$). DataAnalysis software (BrukerDaltonik version 4.2) was used to convert raw spectra to a list of peak locations applying FTMS peak picker with the absolute intensity threshold set to the default value of 100. To further reduce cumulative errors, all sample peak lists within a dataset were aligned to each other prior to formula assignment to eliminate possible mass shifts that would impact formula assignment.

Molecular formula assignment. Chemical formulae were assigned using EMSL software following the compound identification algorithm (CIA), described by Kujawinski and Behn and modified by Minor and colleagues[42]. The following criteria were used for formula assignments: S/N >7, mass measurement error <1 ppm, and C, H, N, O, S, and P were the only elements considered. The presence of P cannot be confirmed through isotope analogues in the same way as the other elements. Therefore, P was only included in formulae where a single P atom was accompanied by at least four O atoms and two P atoms by at least seven O atoms. Additionally, we consistently picked the formula with the lowest error and the lowest number of heteroatoms, since molecules containing both P and S are relatively rare. All calculated formulae were screened according to a list of selection criteria previously applied to eliminate those unlikely to occur in natural OM (refs 33,43,44). The possibility for other potential formula assignments within our mass error ranges increases with increasing mass or mass to charge ratios. Thus, peaks with large mass to charge ratios (m/z values >500) often have multiple possible formulae. These peaks were assigned formulae through the detection of homologous series (CH_2, O, H_2). Specifically, whenever an observed $m/z > 500$ could be assigned by adding the m/z of a group (CH_2, O, H_2) consistent with a homologous series to the m/z of an already putative assignment for a smaller compound, the formula for the large compound was assigned in this manner. If no chemical formula matched an m/z value within the allowed error, the peak was not included in the list of elemental formulae (that is, the peak was unassigned).

Organic compound characteristics. The stoichiometry of each assigned formula was used to calculate the nominal oxidation state of C (NOSC) for that compound (see below). Organic compound composition was further examined in van Krevelen diagrams and assigned to major biochemical classes based on the molar

H:C (y-axis) and O:C (x-axis) ratios (Supplementary Table 4)[23–25,45]. We also calculated aromaticity index (AI) (ref. 33), double bond equivalents per C atom (dbe/C) (ref. 33), and number of compounds with or without different heteroatoms (N, S, and P) and averaged these values for non-sulfidic and sulfidic samples, respectively (Supplementary Table 5). Our abundance calculations assumed equal concentrations for all compounds with an assigned molecular formula; in other words, the intensity of the peak was disregarded and a simple presence/absence approach was employed to assign relative abundance. This approach avoids biases incurred by different ionization efficiencies for different types of compounds and potential interferences between compounds or from complexation with metals. In general, the ionization efficiency is determined by the ability of different functional groups to stabilize the charge. In negative ion mode, ESI preferentially ionizes molecules that can carry a negative charge as a result of deprotonation. For example, acidic functional groups, such as carboxylic acids, are easily deprotonated and preferentially ionized relative to alcohols or nitrogen-containing compounds. This leads to charge competition when both compound types are present in an extract. For example, lipid-like compounds with carboxylic functional groups will be more readily ionized than compounds such as lignin, tannins, and sugars, which are rich in hydroxyl functional groups. In general, compound classes ionize in the following order: lipids > lignin > hydrophilic tannins/sugars. In this study, all samples were run under similar conditions, with similar starting concentrations. The effect of noise peaks was minimized by assigning formulae only to peaks with S/N >7. While normalized peak intensities could be used to correlate changes among individual peaks, this information could also be misleading if samples from different regions were included, as in this study. Such comparisons would require considerable replication, as the intensity values could shift between 20 and 30% in technical replicates, and this was beyond the scope of the current study.

NOSC and thermodynamic calculations. All terms used in the equations below are defined in Supplementary Table 2. The nominal oxidation state of carbon (NOSC) (equation (1)) (ref. 13) was calculated based on the elemental stoichiometry of each organic compound identified in the water extracts. The NOSC of individual compounds present in each sample or assigned to a specific compound class (for example, lipids or carbohydrates) was averaged to give the NOSC of soluble organic matter in that sample or belonging to that compound class. This allowed us to evaluate the relevance of thermodynamic limitations by revealing trends in NOSC values between sulfidic and non-sulfidic environments.

$$\text{NOSC} = 4 - \frac{4c + h - 2o - 3n - 2s + 5p - z}{c} \quad (1)$$

The thermodynamic limit for sulfate respiration was defined as the point where the thermodynamic driving force (equation (2)) (ref. 7), F_T, equals zero. We assumed a linear relationship between NOSC and the change in Gibbs free energy for the oxidation of organic carbon (ΔG_{ox}°), as described by LaRowe and Van Capellen[13] (equation (4)).

$$F_T = 1 - \exp\left(\frac{\Delta G_r + m\Delta G_{ATP}}{\chi RT}\right) \quad (2)$$

$$\Delta G_r^\circ = \Delta G_{ox}^\circ + \Delta G_{red}^\circ \quad (3)$$

$$\Delta G_{ox}^\circ = 60.3 - 28.5 \times \text{NOSC} \quad (4)$$

Because the energetic yield is dependent on the concentrations of reactants and products, we also estimated the deviation of ΔG_r from ΔG_r° in our sulfidic sediments (equations (5) and (6)). For this purpose, a simplified reaction (equation (7)) was used to represent the overall metabolic reaction.

$$\Delta G_r = \Delta G_r^\circ + RT \times \ln\left(\frac{[\text{DIC}] \times [HS^-]^a}{[\text{DOC}] \times [SO_4^{2-}]^a \times [H^+]^a}\right) \quad (5)$$

$$a = \frac{4 - \text{NOSC}}{8} \quad (6)$$

$$C_cH_hO_o^- + aSO_4^{2-} + aH^+ \leftrightarrow cHCO_3^- + aHS^- + \frac{h-1}{2}H_2O \quad (7)$$

We used chemical data (Supplementary Table 3) from pore-water samples from the sulfidic zone in Rifle core 753 (565 cm depth), which exhibited among the lowest NOSC values. Dissolved organic C (DOC) and inorganic C (DIC) concentrations (analysed with a Shimadzu TOC-L auto-analyser) were used to represent $C_cH_hO_o^-$ and HCO_3^-, respectively. Sulfate was determined by ion chromatography (Dionex

ICS-2100 equipped with an AS18 analytical column). Sulfide concentrations were determined colorimetrically in a subsample of pore water, which had been immediately preserved with zinc chloride in anoxic vials at the time of collection. The concentration was below the detection limit of $1\,\mu M$ in this particular sample. In fact, all pore-water samples contained <$1\,\mu M$ sulfide, except a few from the Shiprock core, where the sulfide concentrations ranged between 1 and $5\,\mu M$. Here the sulfate concentrations were also very high, 70–110 mM (that is, almost 20 times as high as in the Rifle 753 sample used for the calculations here). Based on this observation the sulfide concentration in the Rifle pore water should not be much lower than the detection limit. Assuming a sulfide concentration of 10 nM puts F_T to 0 at NOSC < −0.3. Higher sulfide concentrations would shift the thermodynamic limit towards more oxidized organic compounds (higher NOSC). For example, 100 nM sulfide (with DOC, DIC, sulfate, and pH values kept constant) corresponds to $F_T = 0$ at NOSC < +0.9, which is considerably above the limit of −0.6 at standard state conditions. Thus, it is reasonable to assume that thermodynamic limitations are indeed responsible for the chemical imprint we observed in our samples.

The amount of thermodynamically preserved organic C in the water exchangeable fraction of sulfidic samples was estimated by multiplying the total amount of water extractable organic C (mg C per kg sediment) with the fraction of compounds with a NOSC < −0.3. The numbers were averaged for all sulfidic samples, and the same calculations were carried out for non-sulfidic samples for comparison.

Statistical analyses. The regional significance of thermodynamic constraints on C oxidation was examined through bivariate linear regression analyses of NOSC of water-soluble organic compounds versus total sulfide and total organic C. For the comparison of organic matter composition a 0.1% total sulfide limit was used to separate sulfidic ($N = 36$) from non-sulfidic ($N = 11$) sediments, and values were averaged within each group. All statistical analyses were carried out in RStudio version 0.98.1103.

Data availability. Data generated for this study are available through the Stanford Digital Repository (http://purl.stanford.edu/vv493cq1169).

References

35. Ravel, B. & Newville, M. ATHENA, ARTEMIS, HEPHAESTUS: data analysis for X-ray absorption spectroscopy using IFEFFIT. *J. Synchrotron Radiat.* **12,** 537–541 (2005).
36. Prietzel, J. *et al*. Sulfur speciation in soil by S K-Edge XANES spectroscopy: comparison of spectral deconvolution and linear combination fitting. *Environ. Sci. Technol.* **45,** 2878–2886 (2011).
37. Cances, B. *et al*. XAS evidence of As(V) association with iron oxyhydroxides in a contaminated soil at a former arsenical pesticide processing plant. *Environ. Sci. Technol.* **39,** 9398–9405 (2005).
38. Noël, V. *et al*. EXAFS analysis of iron cycling in mangrove sediments downstream a lateritized ultramafic watershed (Vavouto Bay, New Caledonia). *Geochim. Cosmochim. Acta* **136,** 211–228 (2014).
39. Heymann, K., Lehmann, J., Solomon, D., Schmidt, M. W. I. & Regier, T. C 1s K-edge near edge X-ray absorption fine structure (NEXAFS) spectroscopy for characterizing functional group chemistry of black carbon. *Org. Geochem.* **42,** 1055–1064 (2011).
40. Wan, J., Tyliszczak, T. & Tokunaga, T. K. Organic carbon distribution, speciation, and elemental correlations within soil microaggregates: applications of STXM and NEXAFS spectroscopy. *Geochim. Cosmochim. Acta* **71,** 5439–5449 (2007).
41. Solomon, D. *et al*. Carbon (1s) NEXAFS spectroscopy of biogeochemically relevant reference organic compounds. *Soil Sci. Soc. Am. J.* **73,** 1817–1830 (2009).
42. Minor, E. C., Steinbring, C. J., Longnecker, K. & Kujawinski, E. B. Characterization of dissolved organic matter in Lake Superior and its watershed using ultrahigh resolution mass spectrometry. *Org. Geochem.* **43,** 1–11 (2012).
43. Stubbins, A. *et al*. Illuminated darkness: molecular signatures of Congo River dissolved organic matter and its photochemical alteration as revealed by ultrahigh precision mass spectrometry. *Limnol. Oceanogr.* **55,** 1467–1477 (2010).
44. Kujawinski, E. B. & Behn, M. D. Automated analysis of electrospray ionization fourier transform ion cyclotron resonance mass spectra of natural organic matter. *Anal. Chem.* **78,** 4363–4373 (2006).
45. Šantl-Temkiv, T. *et al*. Hailstones: a window into the microbial and chemical inventory of a storm cloud. *PLoS ONE* **8,** e53550 (2013).